High Levels of Electrochemical Doping of Carbon Nanotubes: Evidence for a Transition from Double-Layer Charging to Intercalation and Functionalization

Peter M. Rafailov,*,† Christian Thomsen,‡ Urszula Dettlaff-Weglikowska,§ and Siegmar Roth§

Georgi Nadjakov Institute of Solid State Physics, Bulgarian Academy of Sciences, 72 Tzarigradsko Chaussee Blvd., 1784 Sofia, Bulgaria, Institut für Festkörperphysik, Technische Universität Berlin, Hardenbergstrasse 36, 10623 Berlin, Germany, and Max-Planck-Institut für Festkörperforschung, Heisenbergstrasse 1, 70569 Stuttgart, Germany

Received: October 8, 2007; In Final Form: February 4, 2008

We studied the transition from the electrochemical double-layer charging regime to intercalative doping of bundled single-walled carbon nanotubes (SWNT) in KCl and HCl aqueous solution. For this purpose we used high doping levels by applying constant potentials above 1000 mV approaching and slightly exceeding the oxidation potential for Cl^- ions. At each potential in situ Raman measurements of the radial breathing mode (RBM), the high-energy tangential mode (HEM), and the disorder-induced (D) mode were performed. Furthermore, the conductivity and reflectivity of a set of SWNT samples were measured as a function of doping and subsequently the samples were examined by X-ray photoelectron spectroscopy (XPS). From a comparative analysis of the results we conclude that above 1000 mV a significant penetration of chlorine species into the interstitial channels of the SWNT bundles and possible covalent functionalization take place.

1. Introduction

Single-walled carbon nanotubes (SWNT) are remarkable nanostructures with promising perspectives for application as charge storage devices,[1,2] actuators,[3] and various electronic devices.[4] Plenty of these applications are related to doping of SWNTs as their electronic and mechanical properties are very sensitive to charge transfer. For instance, the resistivity of a semiconducting SWNT can be varied over many orders of magnitude upon electrostatic gating or gas absorption, which implies applications such as SWNT-FETs[5] or electrochemical sensors.[6]

Functionalization provides a combination of doping with selective modification of the chemical properties of SWNTs as solubility and reactivity with certain compounds.[7] Attachment of appropriate functional groups dramatically increases the solubility of the nanotube material.[8,9] Sidewall functional groups can react with polymers and improve the mechanical properties of nanocomposites.[10] Organic molecules can be coupled with functionalized nanotubes for sensor applications. Specific functionalization involving covalent bonds can create cross-links between SWNTs to form complex nanotube networks.[8] However, covalent bonds lead to a localization of the nanotube electronic states thus lowering the concentration of free charge carriers in contrast to doping. The high sensitivity of the nanotube electronic structure to doping and functionalization makes Raman spectroscopy a powerful and favored tool to examine the related phenomena in detail.

There are several ways to dope carbon nanotubes. A high degree of charge transfer can be achieved by intercalation, as the guest species in the interstitial channels form a stable charge-transfer compound with the SWNT ropes.[11] On the other hand, a finer tuning of the added charge in the SWNTs can be accomplished electrochemically by varying the potential at their contact interface with an electrolyte solution.[3,12,13] In this case, the electrolyte ions do not readily penetrate the SWNT ropes. Instead, during the initial stages of electrochemical doping in potentiostatic mode, they form a charged double layer only with the external surface of the ropes.[3,12−15] This is of key importance for SWNT applications as actuators, because SWNT expansion or contraction can be related to the transferred charge, which in the double-layer model can be calculated from the applied voltage.[12,13] On the other hand, intercalation can also be performed electrochemically when galvanostatic mode is applied.[16] This regime combined with Raman scattering and impedance spectroscopy was used to study the insertion mechanism of bisulfate ions[17] and alkali metals[16,18] into SWNTs.

Electrochemistry is thus a convenient tool to study doping and functionalization, as it can be applied in both the double-layer and the intercalative regime and can be used for adsorption and covalent bonding[18−20] as well, depending on the electrolyte species. However, still little is known about the transition from double-layer charging to the intercalative regime.

Here we report an in situ Raman investigation of the electrochemical response of SWNT ropes exposed to potentials above 1000 mV in aqueous solutions of KCl and HCl. We utilize the relatively low oxidation potential of chloride ions in aqueous solutions so that one can successively observe double-layer charging below 1000 mV and electrolytic reactions with significant faradaic current above 1000 mV. Combining our Raman evidence with results from infrared reflectance, XPS, and conductivity measurements, we show that these processes lead to intercalation and functionalization of the SWNTs which can be possibly monitored by Raman spectroscopy.

2. Experimental Section

A stripe of laser-ablation grown "buckypaper'' (MPI-Stuttgart) with a SWNT diameter distribution ranging from 1.25 to

* Corresponding author. E-mail: rafailov@issp.bas.bg.
† Bulgarian Academy of Sciences.
‡ Technische Universität Berlin.
§ Max-Planck-Institut für Festkörperforschung.

10.1021/jp709830y CCC: $40.75
Published on Web 04/05/2008

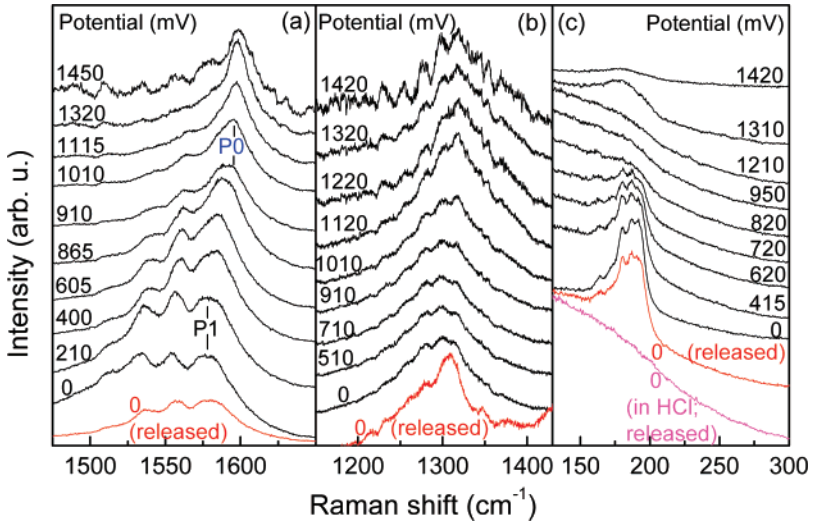

Figure 1. Raman spectra at 1.92 eV excitation energy of the high-energy mode (HEM) (a), the disorder-induced (D) mode (b), and the radial breathing mode (RBM) (c) at several elevated potentials in 1 M KCl. The red traces marked with "released" were obtained after releasing the applied potential from its maximal value down to 0 mV. The lowest trace in (c) was obtained after releasing the potential to 0 mV in 1 M HCl.

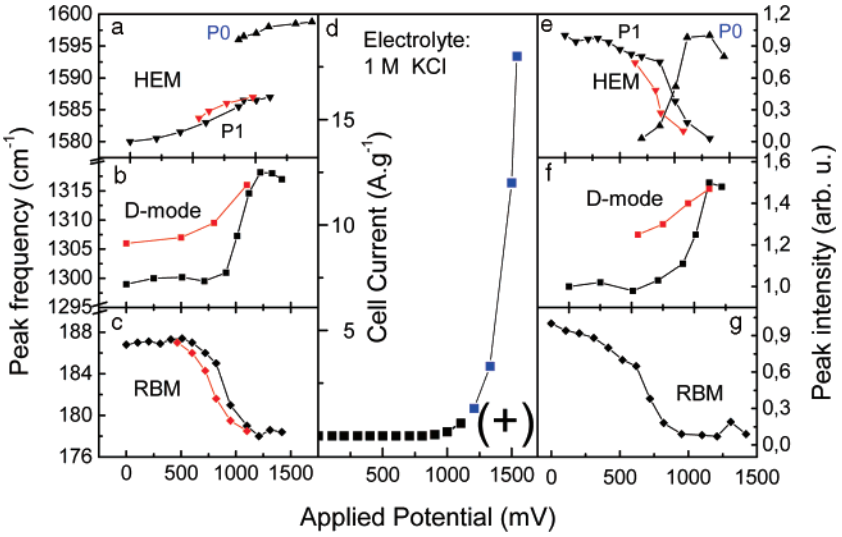

Figure 2. Left: comparative plot of the doping-induced frequency shifts of the HEM (a), D-mode (b), and the RBM (c). Middle (d): the specific current flowing through the electrochemical cell vs the applied potential in anodic polarization. (+): At higher potentials above 1100 mV the cell was operated in galvanostatic mode. The blue points in the graph represent the applied current values. Right: comparative plot of the doping-induced intensity changes of the HEM (e), D-mode (f), and the RBM (g). In all graphs the red points reflect values obtained upon releasing the potential from its maximal value down to 0 mV. Curves connecting experimental points are only guides to the eye.

1.45 nm and a surface density of about 10^{-5} g/mm^2 was prepared as a working electrode in a three-electrode cell equipped with quartz windows. The measurements were carried out using a Metrohm three-electrode potentiostat. A platinum wire and Ag/AgCl served as auxiliary and reference electrode, respectively. The working electrode was dipped for its most part into the solution (1 M aqueous solution of KCl and HCl) and was electrically contacted at its dry end. The double-layer capacitance of the working electrode was measured by cyclic voltammetry[15] and found to be about 35 F/g. At the beginning of the measurement series the working electrode was cycled several times between 400 and −400 mV to ensure a maximum degree of wetting and to remove oxygen-containing functionalities possibly adsorbed on the SWNT sidewalls. The electrolyte solutions were purged with N_2 gas prior to the measurements to remove dissolved oxygen. All chemicals used were of analytical grade quality. The solutions were prepared using doubly distilled water.

The nanotube electrode was polarized anodically in order to utilize the relatively low oxidation potential of chloride ions (1140 mV vs Ag/AgCl). Oxidation of water molecules on carbon electrodes in alkali chloride solutions is normally shifted to higher potentials due to a high overvoltage. Therefore, one can safely assume that possible electrolytic reactions at potentials of 1100−1500 mV comprise predominantly oxidation of Cl^-. Above 1200 mV a formation of gas bubbles commenced with increasing strength which made it impossible to proceed with the Raman monitoring above 1500 mV. The SWNTs were doped in the potentiostatic mode, and Raman spectra were measured in situ at the end of each potential step after waiting for the cell current to decrease below 5 mA/g to ensure quasi-equilibrium conditions.[18] (Quotation in A/g units means specific current, i.e., current normalized to the mass of active electrode material.) Due to the significant current flowing above 1000 mV, the exact determination of the applied potential was difficult; therefore, from 1100 mV the cell was operated in galvanostatic mode, the corresponding constant current flowing through the cell for 20 min in each single experiment. To ensure connexity of the layout, potential values above 1100 mV are quoted as approximate estimates in what follows.

An Ar^+/Kr^+ laser (1.92 eV) was used for excitation. The Raman spectra were recorded with a Dilor triple-grating spectrometer equipped with a CCD detector. The spectrometer was calibrated in frequency using a neon lamp and the laser plasma lines. The infrared measurements were performed with a Bruker IFS 66 spectrometer using globar illumination source. The conductivity measurements were done by the four-probe method.

The XPS measurements were carried out in the UHV chamber of the electron spectrometer ESCALAB-MkII (VG Scientific Ltd.) with a base pressure of 1×10^{-8} Pa. The photoelectron spectra were excited with the Mg Kα radiation (1253.6 eV) with a total instrumental resolution of ~1 eV. The C1s, Cl2p, and O1s photoelectron lines were recorded. All spectra were calibrated by using the C1s line centered at 285 eV.

3. Results and Discussion

Figure 1 shows Raman spectra of the main three vibrational bands of SWNTs at several elevated potentials. The chosen laser excitation is in resonance with the first optical transition of metallic SWNTs; therefore, the high-energy tangential mode (HEM) in the undoped state has a broadened line shape with resonantly enhanced peaks from metallic nanotubes on its low-frequency side. Initially, all phonon frequencies exhibit only slight linear upshifts with doping up to 700 mV, except the HEM features from metallic SWNTs, which are very sensitive to doping.[21,22] Their phonon frequencies are softened in the undoped state due to a Kohn anomaly; therefore, the removal of this anomaly upon doping leads to a dramatic intensity redistribution within the HEM which enhances the higher-frequency peaks of this band.[22] The initial slight upshift of all phonons is well described within the double-layer charging regime of electrochemical doping.[12−15,23] However, upon further potential increasing all modes undergo strongly nonlinear jumps in frequency and intensity. The HEM undergoes a further intensity redistribution connected with replacing of the main HEM peak P1 (≈1585 cm^{-1}) by a new peak P0 (≈1595 cm^{-1}) which is absent in undoped SWNTs (Figure 1a).

The radial breathing mode (RBM) undergoes simultaneously a dramatic drop and a redistribution of its scattering intensity (Figure 1c). In doping experiments this normally occurs upon penetration of intercalating species into the SWNT bundles. Interestingly, this intensity redistribution appears as an overall softening of the RBM band by a considerable amount (about 8 cm^{-1} or 5% of its original frequency). In the following discussion we will comment on this issue in detail.

The disorder-induced (D) mode exhibits a considerable increase in frequency and intensity in going from 900 to 1200 mV (Figure 1b). In graphite and carbon nanotubes the D-mode intensity is generally proportional to the defect density. As covalent functionalization leads to a local disruption of the sp^2-bonded nanotube-wall network, D-band intensity growth is normally observed upon functionalization[24,25] and, especially, in its initial stages.[26] Even the mere population of the interstitial channels of SWNT bundles with counterions without covalent bonding causes an enhancement of the D-band[18,27] as this brings changes in the local environment of the carbon atoms.

The changes in frequency and intensity of the three main SWNT vibrational bands are presented in Figure 2 together with the cell current as a function of the applied potential. All these changes take place in a strongly correlated manner as can be appreciated from a comparison of Figure 2a−c and Figure 2e−g, respectively, and correspond to the onset of a significant cell current which starts to exponentially increase between 800 and 1200 mV (see Figure 2d). As the oxidation potential for Cl^- ions in aqueous KCl is relatively low, and in view of the high overvoltage for electrolytic dissociation of water, we assume that this current comprises a transport of Cl^- ions toward the anode. Upon discharging the most part of the newly appeared Cl_2 molecules emerge as gas bubbles. However, a bundle penetration and adsorption of even a small amount of chlorine species onto the nanotube walls can explain the presented Raman observations. Additionally, Figure 2 shows that the Raman bands exhibit a markedly hysteretic behavior of both their frequencies and intensities, thus giving evidence for a significantly stronger interaction and charge transfer with the nanotubes than is expected within the double-layer model. However, we found the hysteresis of all bands to strongly depend on the sample history and the highest potential reached U_{max}, with large hysteresis for $U_{max} > 1300$ mV and perfect reversibility for a fresh sample and $U_{max} \leq 800$ mV.

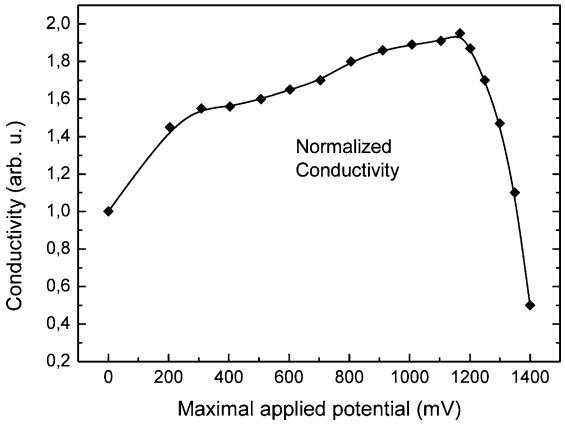

Figure 3. Normalized dc conductivity of the SWNT working electrode vs maximal applied potential in 1 M KCl. The displayed values are normalized to the conductivity of the undoped sample.

To gain further insight into the electrochemical doping processes with SWNTs beyond the double-layer regime we measured the conductivity and the reflectivity of our samples. The dc conductivity was measured by the four-probe method on a set of samples after each sample was polarized as working electrode to a different maximal potential U_{max} and then dried in an inert atmosphere for several days. The functional dependence of the conductivity on this maximal potential is displayed on Figure 3. It is clearly seen from this figure that electrochemical doping with U_{max} up to 1100−1200 mV enhances the SWNT conductivity, but further potential increase causes it to steeply drop even below the undoped sample value. Similar evidence is obtained from Figure 4 where far-infrared reflectance spectra of the SWNT electrodes polarized to different U_{max} are displayed: reflectivity follows virtually the same potential dependence as the conductivity.

Our explanation for the observed effects is as follows: on approaching the oxidation potential of Cl^- ions (1140 mV vs Ag/AgCl) increasingly more Cl^- ions tunnel through the double layer and discharge on the SWNT anode, some of them penetrating into the SWNT bundles. The newly created chlorine atoms remain for a short time adsorbed on the SWNT walls until they form a Cl_2 molecule with another discharged Cl^- ion. Due to the acceptor behavior of chlorine this physisorption leads to a much larger charge transfer with the nanotube than is possible in the double-layer regime. Therefore, the loss in the RBM and HEM intensity (see Figure 2, parts e and f) can be ascribed to a loss of resonance upon depleting the first optical transition of metallic SWNTs.

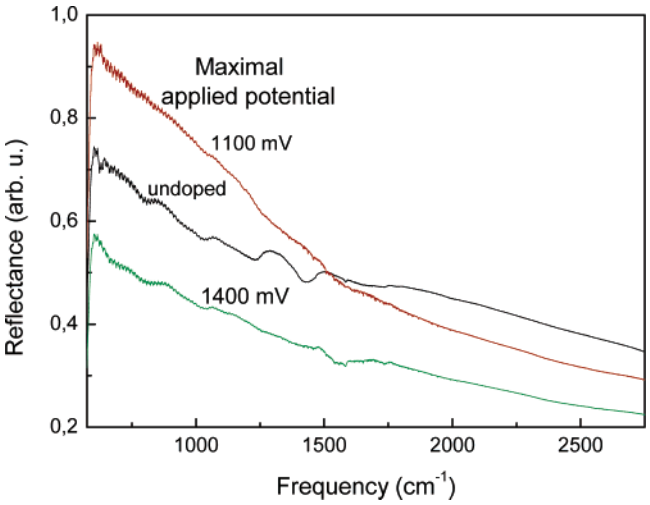

Figure 4. Far-IR reflectance spectra of SWNT samples polarized to different maximal potentials in 1 M KCl.

The RBM behavior beyond the double-layer regime deserves special discussion as this band undoubtedly exhibits the most complicated response to the applied high-potential electrochemical attack. In our opinion, the observed RBM behavior is governed by a subtle interplay of three main factors:

(i) The doping-induced depletion of resonant electronic transitions is diameter-dependent (smaller-diameter tubes lose resonance at higher doping levels than wider ones[12]).

(ii) The reactivity toward covalent bond formation depends on the diameter and on the electronic structure (again, smaller-diameter tubes being more reactive than wider ones,[28] and metallic tubes being more reactive than semiconducting ones[29]). In this case, however, the chemical reaction damages the delocalized nanotube electronic structure thus bringing the functionalized SWNTs out of resonance.

(iii) SWNT-bundle morphology changes upon penetration of electrolyte species leading to changes in transition energies[26] and to a partial debundling which decreases the additional RBM force constant coming from the intertube van der Waals interaction.[30,31]

Last but not least, the Raman efficiency of the RBM in an individual SWNT increases with decreasing diameter.[32]

The experimentally observed behavior of the RBM band implies that factors ii and iii have a prevailing influence because factor i alone would lead to an apparent blue shift of the band.[12] Unfortunately, the effects due to (ii) and (iii) cannot be correctly quantified separately. Such a quantification would be perhaps possible with measurements at several different wavelengths, as was pointed out in ref 33, and on samples of HiPco nanotubes where individual SWNTs are spectroscopically traceable.[34,35] The authors of ref 34 were therefore able to derive the so-called "resonance rule" thus explaining the apparent differences in the spectroscopically detected sensitivity of individual nanotubes to electrochemical doping.[34,35] The laser-ablation grown SWNTs in our sample have relatively large diameters with a narrow distribution and hence close-together-lying electronic transitions. Therefore, their spectral features behave in a more unified manner yielding the apparent red shift of the RBM band as a whole which essentially comprises an intensity redistribution and, probably to a lesser extent, softening of the RBMs of individual tubes caused by partial debundling. After saturation of the RBM dependence on the applied potential above 1250 mV (see Figure 1c) it may be assumed that the vast majority of SWNTs have largely lost their Raman resonance. It is then interesting to make a qualitative check if the RBM band envelope reflects the diameter distribution in the sample applying the experimentally determined relation $\omega_{RBM} = c_1/d + c_2$, ($d$ being the nanotube diameter, $c_1 = 215$ cm^{-1}·nm, and $c_2 = 18$ cm^{-1}).[36] Using peak frequency of 178 cm^{-1} and line width (fwhm) of 30 cm^{-1} as determined from a Gaussian curve fit (see Figure 1c, uppermost trace), we arrive at a mean diameter of 1.34 nm and a distribution width of 0.13 mn, in good agreement with the producer data.

After Cl_2 molecules are created, a part of them leaves the solution in the form of gas bubbles. Another part reacts with water forming the acids HClO, HCl, and, possibly, other related acids which all are strong oxidizing agents. HClO partially decomposes generating free oxygen, and the presence of HCl lowers the pH value of the solution. Both these processes are known to cause oxidation of conventional graphite electrodes made of, e.g., HOPG,[37,38] or even the more resistant glassy carbon[39]. Thus, the generation of chlorine gas triggers a sequence of reactions that may ultimately lead to considerable oxidation of carbon nanotube walls which essentially comprises formation of various covalent C−O and possibly C−Cl bonds (functionalization). These processes should particularly accelerate above the Cl^- oxidation potential and lead to a localization of the nanotube electronic states thus lowering the concentration of free carriers created by the preceding electrochemical doping and consequently lowering the conductivity and reflectivity of the sample. This explanation is additionally supported by the fact that the major changes in the Raman spectra first appear in the behavior of the RBM which starts to dramatically lose intensity and terminates its linear upshift already at about 750 mV thus signaling a possible onset of penetration into the bundles. The intensity increase of the D-mode reflecting formation of new chemical bonds is the latest process which starts when the potential exceeds 1000 mV. In regard to the HEM, we recall that both peaks P0 and P1 coexist in the HEM between 800 and 1200 mV, P0 gaining intensity from P1, and the HEM shape above 1200 mV resembles that of intercalated or functionalized[29,40] SWNTs. Therefore, our tentative explanation for this observation is that P0 develops from P1 in tubes that have undergone functionalization. These are mainly smaller-diameter SWNTs as inferred from the behavior of the RBM band. Our results thus imply that bundle penetration and functionalization can be possibly controlled by Raman spectroscopy after a suitable calibration to the frequency and intensity of the Raman bands.

To check the pH influence on the Raman response of the SWNT electrode we examined the evolution of the RBM upon anodic polarization up to 1400 mV in 1 M aqueous solution of HCl. We found a much stronger loss in intensity on increasing potential, and the band could not be recovered at all upon releasing potential even to 0 mV (see Figure 1c, lowest trace) indicating a possible irreversible loss of the two-dimensional (2D) order within the bundles.

We further analyzed our samples with X-ray photoelectron spectroscopy (XPS). In Figure 5 XPS spectra of the carbon 1s, chlorine 2p, and oxygen 1s level in SWNT samples polarized to different maximal potentials are presented. Detailed analysis of the XPS spectra provides clear evidence for a chemical modification of the SWNTs upon exposure to high electrochemical potentials. The carbon 1s peak, observed at 285 eV for sp^2 carbon in the pristine sample, moves to lower binding energy, reaching a shift of 0.3 eV for $U_{max} = 1400$ mV, most probably due to the acceptor behavior of the chlorine species attached to the nanotube walls.[8] Furthermore, the shoulder at 286.6 eV corresponding to C−O bonded carbon[41] exhibits a

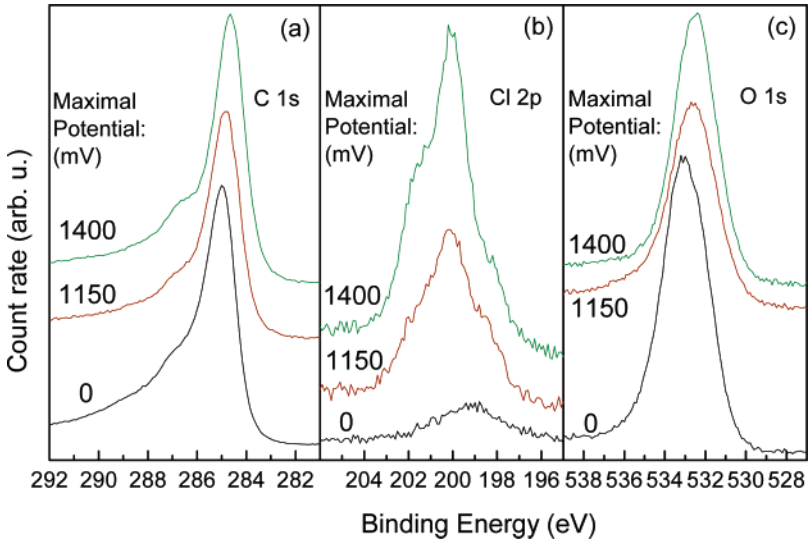

Figure 5. XPS spectra of the carbon 1s (a), chlorine 2p (b), and oxygen 1s (c) level in SWNT samples polarized to different maximal potentials in 1 M HCl as quoted in the graphs. $U_{max} = 0$ mV means only a brief wetting of the sample in the solution without electrical contact.

gain in intensity for $U_{max} = 1400$ mV as compared to $U_{max} = 1150$ mV confirming the activation of oxidation reactions at potentials above 1150 mV. The spectrum of the Cl 2p region shows two doublets suggesting chlorine ionically (198.6 eV) and covalently (200.1 eV) bonded to the SWNTs, respectively.[40] The intensity of the higher-energy doublet increases with the applied potential indicating an increase of the share of covalently bonded (functionalized) Cl. XPS spectra of oxygen reveal also a shift of the O 1s level to lower energies for $U_{max} = 1150$ mV and $U_{max} = 1400$ mV as compared to the undoped sample values ($U_{max} = 0$ mV) suggesting a significant oxidation of the SWNTs promoted by the applied combination of high potentials and currents.

4. Conclusions

Upon electrochemical doping of SWNTs in aqueous chloride solutions a penetration of chlorine species begins into the SWNT bundles above 800 mV. Up to potentials of ≈1100 mV, however, double-layer charging accompanied by physisorption-induced charge transfer is still the prevailing doping process. Above 1100 mV chemical reactions with covalent C−O and C−Cl bond formation increasingly take place, triggered by the creation of Cl_2 gas, leading to an electrochemical functionalization of the SWNTs, the smaller-diameter ones being most strongly affected. The onset and the initial stages of the bundle penetration and the functionalization can be monitored by Raman spectroscopy and possibly controlled after a suitable calibration to the frequency and intensity of the various Raman bands.

Acknowledgment. P.M.R. acknowledges support from the NATO Reintegration Grant No. CBP.EAP.RIG.982322. We thank M. Monev and Ts. Dobrev for fruitful discussions and G. Tyuliev and H. Kolev for completing the XPS measurements.

References and Notes

(1) (1) Liu, C.; Bard, A. J.; Wudl, F.; Weitz, I.; Heath, J. R. *Electrochem. Solid-State Lett.* **1999**, *2*, 577.

(2) Claye, A. S.; Fisher, J. E.; Huffman, C. B.; Rinzler, A. G.; Smalley, R. E. *J. Electrochem. Soc.* **2000**, *147*, 2845.

(3) Baughman, R. H.; Cui, C.; Zakhidov, A.; Iqbal, Z.; Barisci, J. N.; Spinks, G. M.; Wallace, G. G.; Mazzoldi, A.; Rossi, D. D.; Rinzler, A. G.; Jaschinski, O.; Roth, S.; Kertesz, M. *Science* **1999**, *284*, 1340.

(4) Reich, S.; Thomsen, C.; Maultzsch, J. *Carbon Nanotubes: Basic Concepts and Physical Properties*; Wiley-VCH: Weinheim, Germany, 2004.

(5) Tans, S. J.; Verschueren, A.; Dekker, C. *Nature* **1998**, *393*, 6680.

(6) Modi, A.; Koratkar, N.; Lass, E.; Wei, B.; Ajayan, P. M. *Nature* **2003**, *424*, 171.

(7) Balasubramanian, K.; Burghard, M. *Small* **2005**, *1*, 180.

(8) Dettlaff-Weglikowska, U.; Benoit, J.-M.; Chiu, P.-W.; Graupner, R.; Lebedkin, S.; Roth, S. *Curr. Appl. Phys.* **2002**, *2*, 497.

(9) Curulli, A.; Cesaro, S. N.; Coppe, A.; Silvestri, C.; Palleschi, G. *Microchim. Acta* **2006**, *152*, 226.

(10) Dyke, C. A.; Tour, J. M. *J. Phys. Chem. A* **2004**, *108*, 11151.

(11) Rao, A. M.; Eklund, P. C.; Bandow, S.; Thess, A.; Smalley, R. E. *Nature* **1997**, *88*, 257.

(12) Kavan, L.; Rapta, P.; Dunsch, L.; Bronikowski, M. J.; Willis, P.; Smalley, R. *J. Phys. Chem. B* **2001**, *105*, 10764.

(13) Kavan, L.; Dunsch, L. *ChemPhysChem* **2007**, *8*, 974.

(14) An, C. P.; Zardeny, Z. V.; Iqbal, Z.; Spinks, G. G.; Baughman, R. H.; Zakhidov, A. *Synth. Met.* **2001**, *116*, 411.

(15) Stoll, M.; Rafailov, P. M.; Frenzel, W.; Thomsen, C. *Chem. Phys. Lett.* **2003**, *375*, 625.

(16) Claye, A.; Fischer, J. E.; Metrot, A. *Chem. Phys. Lett.* **2000**, *330*, 61.

(17) Sumanasekera, G. U.; Allen, J. L.; Fang, S. L.; Loper, A. L.; Rao, A. M.; Eklund, P. C. *J. Phys. Chem. B* **1999**, *103*, 4292.

(18) Claye, A.; Rahman, S.; Fischer, J. E.; Sirenko, A.; Sumanasekera, G. U.; Eklund, P. C. *Chem. Phys. Lett.* **2001**, *333*, 16.

(19) Bahr, J. L.; Yang, J.; Kosynkin, D. V.; Bronikowski, M. J.; Smalley, R. E.; Tour, J. M. *J. Am. Chem. Soc.* **2001**, *123*, 6536.

(20) Unger, E.; Graham, A. A.; Kreupl, F.; Liebau, M.; Hoenlein, W. *Curr. Appl. Phys.* **2002**, *2*, 107.

(21) Piscanec, S.; Lazzeri, S.; Robertson, J.; Ferrari, A. C.; Mauri, F. *Phys. Rev. B* **2007**, *75*, 035427.

(22) Rafailov, P. M.; Maultzsch, J.; Thomsen, C.; Kataura, H. *Phys. Rev. B* **2005**, *72*, 045411.

(23) Rafailov, P. M.; Stoll, M.; Thomsen, C. *J. Phys. Chem. B* **2004**, *108*, 19241.

(24) Hu, H.; Zhao, B.; Hamon, M. A.; Kamaras, K.; Itkis, M. E.; Haddon, R. C. *J. Am. Chem. Soc.* **2003**, *125*, 14893.

(25) Wang, C.; Cao, Q.; Ozel, T.; Gaur, A.; Rogers, J. A.; Shim, M. *J. Am. Chem. Soc.* **2005**, *127*, 11460.

(26) Graupner, R. *J. Raman Spectrosc.* **2007**, *38*, 673.

(27) Kim, Y. A.; Kojima, M.; Muramatsu, H.; Umemoto, S.; Watanabe, T.; Yoshida, K.; Sato, K.; Ikeda, T.; Hayashi, T.; Endo, M.; Terrones, M.; Dresselhaus, M. S. *Small* **2006**, *2*, 667.

(28) Banerjee, S.; Wong, S. *Nano Lett.* **2004**, *4*, 1445.

(29) Skakalova, V.; Kaiser, A. B.; Dettlaff-Weglikowska, U.; Hrncarikova, K.; Roth, S. *J. Phys. Chem. B* **2005**, *109*, 7174.

(30) Venkateswaran, U. D.; Rao, A. M.; Richter, E.; Menon, M.; Rinzler, A.; Smalley, R. E.; Eklund, P. C. *Phys. Rev. B* **1999**, *59*, 10928.

(31) Thomsen, C.; Reich, S.; Goni, A. R.; Jantoljak, H.; Rafailov, P. M.; Loa, I.; Syassen, K.; Journet, C.; Bernier, P. *Phys. Status Solidi B* **1999**, *215*, 435.

(32) Machón, M.; Reich, S.; Telg, H.; Maultzsch, J.; Ordejón, P.; Thomsen, C. *Phys. Rev. B* **2005**, *71*, 035416.

(33) Dyke, C. A.; Stewart, M. P.; Tour, J. M. *J. Am. Chem. Soc.* **2005**, *127*, 4497.

(34) Kavan, L.; Kalbáč, M.; Zukalová, M.; Dunsch, L. *J. Phys. Chem. B* **2005**, *109*, 19613.

(35) Kavan, L.; Kalbáč, M.; Zukalová, M.; Dunsch, L. *Phys. Status Solidi B* **2006**, *243*, 3130.

(36) Maultzsch, J.; Telg, H.; Reich, S.; Thomsen, C. *Phys. Rev. B* **2005**, *72*, 205438.

(37) Kinoshita, K. *Carbon—Electrochemical and Physicochemical Properties*; Wiley-Interscience: New York, 1988.

(38) Goldsmith, B. R.; Coroneus, J. G.; Khalap, V. R.; Kane, A. A.; Weiss, G. A.; Collins, P. G. *Science* **2007**, *315*, 77.

(39) Dunsch, L. *Z. Chem.* **1974**, *14*, 463.

(40) Dettlaff-Weglikowska, U.; Skakalova, V.; Graupner, R.; Jhang, S. H.; Kim, B. H.; Lee, H. J.; Ley, L.; Park, Y. W.; Berber, S.; Tomanek, D.; Roth, S. *J. Am. Chem. Soc.* **2005**, *127*, 5125.

(41) Licea-Jimenez, L.; Henrio, P.-Y.; Lund, A.; Laurie, T. M.; Pérez-García, A. A.; Nyborg, L.; Hassander, H.; Bertilsson, H.; Rychwalski, R. W. *Compos. Sci. Technol.* **2007**, *67*, 844.